Catalysis Science & Technology

The nature of the active sites of Pd-Ga catalysts in the hydrogenation of CO_2 to methanol

Journal:	*Catalysis Science & Technology*
Manuscript ID	CY-ART-05-2020-000956.R1
Article Type:	Paper
Date Submitted by the Author:	26-Jul-2020

Complete List of Authors:	Manrique, Raydel; Universidad de Concepcion, Facultad de Ingeniería, Departamento de Ingeniería Química Rodríguez Pereira, Jhonatan; UIS Universidad Industrial de Santander, Laboratorio de Ciencias de Superficies (SurfLab) Rincón, Sergio; Universidad Industrial de Santander, Laboratorio de Ciencia de Superficies Bravo-Suárez, Juan; The University of Kansas, Chemical & Petroleum Engineering Department; The University of Kansas, Center for Environmentally Beneficial Catalysis Baldovino Medrano, Víctor Gabriel; UIS Universidad Industrial de Santander, Centro de Investigaciones en Catálisis; Universidad Industrial de Santander, Laboratorio de Ciencia de Superficies Jiménez, Romel; Universidad de Concepción, Chemical Engineering Karelovic, Alejandro; Universidad de Concepción, Chemical Engineering

The nature of the active sites of Pd-Ga catalysts in the hydrogenation of CO_2 to methanol

Raydel Manrique[a,*], Jhonatan Rodríguez-Pereira[b], Sergio A. Rincón[c], Juan J. Bravo-Suárez[d,e], Víctor G. Baldovino-Medrano[b,c], Romel Jiménez[a,f], Alejandro Karelovic[a,f,g,*]

[a] *Carbon and Catalysis Laboratory (CarboCat), Department of Chemical Engineering, Universidad de Concepción, Chile.*

[b] *Centro de Investigaciones en Catálisis, Escuela de Ingeniería Química, Universidad Industrial de Santander, Colombia.*

[c] *Laboratorio Central de Ciencia de Superficies, Universidad Industrial de Santander, Colombia.*

[d] *Chemical & Petroleum Engineering Department, The University of Kansas, Lawrence, KS, USA.*

[e] *Center for Environmentally Beneficial Catalysis, The University of Kansas, Lawrence, KS, USA.*

[f] *Unidad de Desarrollo Tecnológico (UDT), Universidad de Concepción, Chile.*

[g] *Millennium Nuclei on Catalytic Processes towards Sustainable Chemistry (CSC), Chile.*

**E-mail: rmanrique@udec.cl, akarelov@udec.cl*

Abstract

The hydrogenation of CO_2 to methanol is a viable alternative for mitigating greenhouse gases net emissions as well as a route for hydrogen storage and transportation. In this work, we studied the nature of the active sites generated by the promotion of Pd with Ga and the surfaces species and their reactivity under reaction conditions, in the hydrogenation of CO_2 to methanol. SiO_2-supported Pd and Pd-Ga catalysts with different Pd/Ga molar ratios were synthesized. Results show that in a narrow interval of Pd/Ga molar ratio (0.5 to 1) the methanol formation rates increased by up to two orders of magnitude compared to non promoted Pd. Interestingly, CO formation rates were barely changed, which resulted in a high selectivity (60% at 800 kPa and 280°C). Characterization by quasi in situ XPS, XRD, CO adsorption DRIFTS and TEM-EDS demonstrate that the primary cause for the increase in activity towards methanol synthesis is the formation of intermetallic compounds such as Pd_2Ga, rather than a cooperative mechanism between Pd and Ga_2O_3. The variation of the Pd/Ga ratio defines the surface concentration of Ga_2O_3, where the deposition of excess Ga in its oxidized form on the mono or bimetallic (Pd or Pd-Ga) phases of the catalysts inhibits their catalytic performance. Additionally, operando DRIFTS characterization showed the formation of bidentate formate species (b-HCOO) on the metallic Pd or Pd-Ga sites acting as intermediates in the hydrogenation of CO_2 to methanol. Unlike methanol, CO formation rate is mainly dependent on the amount of surface metallic sites, irrespective of their nature (Pd or Pd-Ga). Results show that the presence of PdGa intermetallic compounds is necessary to improve the methanol formation rate of Pd-Ga/SiO_2 catalysts.

Introduction

It has been widely recognized that product yields in numerous catalytic reactions can be significantly improved in catalysts consisting of supported monometallic nanoparticles by the addition of secondary metals [1-4]. Such promoted metal catalysts have generated interest in different chemical reactions due to the net improvement in the selectivity to various reaction pathways [1, 3]. This is the case for the synthesis of methanol from CO_2 and H_2 mixtures (Eq. 1). This reaction represents a viable alternative to mitigate net greenhouse gas emissions while exploring routes for energy generation of low environmental impact. Although CO_2 is generally considered a waste product, it can be a sustainable source of carbon for fuel synthesis. Since hydrogen can also be generated from sustainable sources, the hydrogenation of CO_2 to methanol is an interesting alternative to support the methanol economy that can provide energy storage derived from non-fossil fuels [5].

$$CO_2 + 3H_2 \leftrightarrows CH_3OH + H_2O;\ \Delta H^o_{298} = -47\ kJ\ mol^{-1} \quad (1)$$

A competing reaction during methanol synthesis from CO_2/H_2 is the reverse water-gas shift reaction (r-WGS) (Eq. 2), an endothermic reaction which is thermodynamically favored at high temperatures. One of the current challenges in the CO_2 to methanol process is the suppression of the r-WGS reaction and the increase in the turnover frequency (TOF) for the formation of methanol [1, 6, 7]. Such situation would allow operation at lower temperatures where the process can proceed with higher selectivity and greater energy efficiency. For such a purpose, it is necessary to understand the nature of catalyst active sites used in the synthesis of methanol from CO_2/H_2.

$$CO_2 + H_2 \leftrightarrows CO + H_2O;\ \Delta H^o_{298} = 41\ kJ\ mol^{-1} \quad (2)$$

The use of promoters in Cu and Pd based catalysts has been reported to increase the activity and selectivity in the synthesis of methanol from the hydrogenation of carbon dioxide [8-10]. For example, Fujitani et al. [11] studied the effect of different promoters on palladium catalysts and found that Pd/Ga_2O_3 showed the best selectivities and TOF for methanol formation. Several studies have also shown that Pd catalysts promoted with Ga provided high activity and selectivity for the hydrogenation of CO_2 to methanol [12, 13]. In general, there appears to be two main proposed causes that determine the activity of promoted Pd towards methanol. The first mechanistic proposal for promotion is a synergistic effect between the metal and oxides such as Ga_2O_3 [13] and In_2O_3 [14]. In the case of Ga_2O_3, it has been proposed that the synergy is related to the spillover phenomenon, which consists of a rapid chemisorption and dissociation of H_2 on metallic palladium sites favoring a greater migration of hydrogen atoms to Ga_2O_3 where CO_2 hydrogenation to methanol occurs via adsorbed intermediate species [12, 13]. In the case of In_2O_3 promotion, the existence of a synergistic effect between the metal oxide (i.e., In_2O_3) promoter and intermetallic Pd-Metal (e.g., Pd-In) was proposed by Snider et al. [14]. These authors also suggested that oxygen vacancies can form in In_2O_3 that can activate CO_2 molecules. These two hypotheses identified the oxidized phase that coexists with surface mono or bimetallic Pd as a necessary element for the enhancement of activity and selectivity towards methanol. The second mechanistic proposal for promotion in Pd based bimetallic materials for methanol synthesis from CO_2/H_2 is the

formation of intermetallic sites such as Pd_2Ga on Pd-Ga/SiO_2 catalysts, which are proposed to improve the turnover frequency for methanol synthesis [15]. This latter report showed that the activity of Pd-Ga/SiO_2 towards methanol formation was similar to the activity observed in a commercial catalyst (Cu/ZnO/Al_2O_3), while the unwanted production of CO via r-WGS was lower. This proposal [15] coincided with that of other authors who identified an increase in the activity towards the formation of methanol using palladium based catalysts promoted by gallium which suggested that the reason for this phenomenon was the modification of the electronic structure of Pd to form intermetallic phases [16, 17]. While significant research has been done on the synthesis of CH_3OH with Cu and Pd catalysts promoted with secondary metals, to date, little is known about the reaction mechanism on intermetallic Pd catalysts. However, it is worth noting that, on these materials, formate (HCOO*) species have been widely reported as likely reaction surface intermediate species [18-20].

Here, we rigorously study the promotion of palladium particles with Ga by synthesizing a series of Pd/SiO_2 and Pd-Ga/SiO_2 catalysts with different Pd/Ga molar ratios, namely, 0.2, 0.5, 1.0, 2.0, and 4.0, while keeping constant the loading of palladium. The catalytic performance of the catalysts was assessed in terms of their intrinsic activity, selectivity, and stability. Also, we used a combination of complementary techniques to characterize the structure of the catalysts after activation and during the reaction: Quasi in situ X-ray photoelectron spectroscopy (XPS), X-ray diffraction (XRD), in situ diffuse reflectance Fourier-transform spectroscopy (DRIFTS) for CO probe adsorption and operando modes and transmission electron microscopy with electron dispersive X-ray spectroscopy (TEM-EDS). The collected evidence allowed us to conclude that the presence of bimetallic Pd-Ga phases is necessary to increase the rate of methanol formation. The role of residual Ga_2O_3 is mainly to block the active sites (Pd or PdGa) and inhibit the activity of the catalysts. However, it is not possible to discard a synergistic effect between PdGa and gallium oxide, as evidenced recently for the Pd-In system[14]. On the other hand, the rate of CO formation correlated with the available mono- or bi-metallic surface (Pd-Ga or Pd), however, the formation of methanol was more favorable for the bimetallic catalysts.

1. Experimental

1.1 Catalysts preparation

Pd-Ga catalysts were synthesized using SiO_2 as a support. The catalysts were classified as: Pd and Pd/Ga(x), where the x represents the Pd/Ga molar ratio (0.2, 0.5, 1.0, 2.0, or 4.0). The loading of Pd (4.5 wt.%) was kept the same for all of the catalysts. The synthesis of the catalysts was carried out by incipient wet impregnation using $Pd(NO_3)_2$ (≥ 99.0%, Merck) and $Ga(NO_3)_3 \times H_2O$ (≥ 98.0 %Merck) as the Pd and Ga precursor respectively, with addition of triethanolamine (TEA, ≥ 99.0%, Merck) and nitric acid (HNO_3 (aq.) ≥ 65.0% Merck), using a procedure similar to that described by Soled et al. [21]. SiO_2 support was provided by Saint-Gobain NorPro (SS 61138) with sieved particle sizes between 180 and 350 μm, a BET surface area of 230 m^2/g, an average pore diameter of 127 Å, and an average pore volume of 1.09 cm^3/g. This material was chosen as the support because it has a high surface area, it is amorphous, it facilitates the structural analysis of the nanoparticles supported in TEM studies, and it is chemically inert for CO_2 hydrogenation hence allowing a direct comparison

of the catalytic performance of the supported nanoparticles. During the synthesis process, Ga and Pd precursors as well as HNO_3 and TEA were mixed in the appropriate amounts (Table S1) and added dropwise to the support under continuous stirring. The dissolution of the Pd precursor was facilitated using a sonicator. The impregnated samples (ca. 1 g) were dried at 100 °C for 24 h in static air in a drying oven and then calcined at 450 °C in a fixed bed reactor (heating rate of 2 °C/min) for 2 h under a flow of dry air (50 NTP cm^3/min). Then, the catalyst temperature was brought to 30 °C and then it was reduced at 400 °C (Pd) at a heating rate of 2 °C/min for 2 h under a flow of H_2 (99.999%, 50 NTP cm^3/min) [22]. In order to achieve intermetallic Pd-Ga phases, Pd/Ga(x) catalysts were reduced under a flow of H_2 (99.999%, 50 NTP cm^3/min) at 500 °C for 2 h (heating rate 2 °C /min from 25 °C) [17].

1.2 Catalysts characterization

The dispersion of Pd was determined by chemisorption of O_2 following the method of Benson et al. [2, 4]. The dissociative chemisorption of O_2 was measured on a thermogravimetric analyzer (Cahn – Versatherm) with a sensitivity of 0.1 μg. The sample (25 mg) was purged with Ar at 30 °C for 10 min and afterwards reduced in a flow of pure H_2 (100 NTP cm^3/min) at 400 °C (heating rate 2 °C/min) for 2 h. Then, the temperature was lowered to 100 °C under a flow of Ar (100 NTP cm^3/min) to achieve the elimination of hydrogen adsorbed on the surface. Finally, the chemisorption of O_2 was carried out under a flow of dry air (100 NTP cm^3/min) for 30 min at 100 °C. At this temperature, O_2 reacts selectively with the atoms of Pd on the surface with negligible bulk oxidation [23]. The consumption of O_2 was determined by mass difference. A stoichiometry of O/Pd = 1 was assumed for dispersion calculations [23]. This method was not applied to the catalysts promoted by Ga because in this case the stoichiometry for oxygen adsorption is unknown. The dispersion was defined as the ratio between the surface atomic palladium and total Pd atoms in the catalyst. The average size of the particles of palladium was estimated assuming that the particles have a hemispherical shape, thus using Eq. 3:

$$d_p = 6\frac{(v_m/a_m)}{D} \quad (3)$$

Where, v_m is the volume of a single metallic atom in the bulk (14.7 $Å^3$), a_m is the area of a single metallic atom on the surface (7.93 $Å^2$), and D is the fractional dispersion of Pd.

The morphology and particle size distribution of the metal particles in the supported catalysts were determined by transmission electron microscopy (JEOL JEM-1200 EX II). The average sizes of metal particles were calculated in this work as the average diameter in number ($\bar{d}$) defined in Eq. 4.[24].

$$\bar{d} = {\sum_i n_i d_i}\Big/{\sum_i n_i} \quad (4)$$

Where, n_i is the number of particles of d_i diameter and $\sum_i n_i$ is the number of analyzed nanoparticles.

Additionally, images were obtained from transmission electron microscopy with spectroscopic mapping by energy dispersion X-ray spectroscopy (EDS) using an FEI TECNAI F20 XT transmission electron microscope equipped with a field emission gun and operated at an acceleration voltage of 200 kV. The diameter of the probe used for the experiments was 0.25 nm.

Bulk crystalline phases were analyzed by measuring the XRD patterns of the catalysts using a Bruker D4 diffractometer provided with CuKα radiation (λ = 0.154 nm). The 2θ range was scanned between 3 and 90° at a speed of 0.02°/s. The identification of the crystalline phases was done by a search-match procedure with the software Mercury 3.7 using the COD database [25]. Also, the sizes of the metallic particles in the supported catalysts were estimated by the Scherrer equation [26].

The surface chemical state of the catalysts was measured by quasi in situ XPS using the XPS/ISS/UPS-A. Centeno surface characterization platform built by SPECS (Germany). The platform is provided with a PHOIBOS 150 2D-DLD energy analyzer package. A monochromatized X-ray source Al-Kα (FOCUS 500) operated at 200W was employed for the measurements. The pressure in the analysis chamber was approximately 1×10^{-7} Pa. The pass energy of the hemispheric analyzer was set to 60 eV for recording high-resolution spectra. Previous to the analyses, samples were pre-treated using a high-pressure cell (HPC) coupled with the XPS analysis chamber, hence allowing to analyze the samples directly after the applied pre-treatments and avoiding contact with ambient air. The general procedure was as follows: the samples recovered after the catalytic tests were placed in the HPC, and three different treatments were applied sequentially with the collection of XPS spectra right after each treatment. The applied treatments were (at 101 kPa): i) Reduction under H_2 flow (50 NTP cm^3/min) at 500 °C (heating rate: 5 °C/min) and then oxidation with oxygen flow (20 NTP cm^3/min) at 25 °C; ii) Reduction in H_2 flow (50 NTP cm^3/min) at 500 °C (heating rate: 5 °C/min); and iii) Reduction with H_2 (50 NTP cm^3/min) at 500 °C (heating rate 5 °C/min) with subsequent emulation of reaction conditions (260 °C, 40 NTP cm^3/min H_2/CO_2 = 3). During the XPS analyses, the surface charge compensation of the samples was controlled with a flood gun device (FG 15/40-PS FG500) operated at 70 μA and 3.5 eV. High-resolution spectra were recorded for the following core levels: C 1s, O 1s, Na 1s, Si 2s, Ga 2p, and Pd 3d. The stability of the surface charge compensation was verified by recording the C 1s peak at the end of the analysis. Data analysis was performed with the CasaXPS program (Casa Software Ltd) using the SPECS Prodigy library for R.S.F. values. A U 3 Tougaard baseline[27] was employed for background modeling together with a 70% Gaussian - 30% Lorentzian line shape for peak decomposition. The binding energy (BE) scale of the spectra was corrected taking the Si component of the Si 2p peak at 103.5 eV as a reference.

1.3 Catalytic activity measurements

The performance of the catalysts was evaluated using a fixed-bed reactor system. Catalysts were loaded into a stainless-steel tube with an internal diameter of 7.8 mm placed in an electric oven. The gases, H_2 and CO_2, were provided by Air Liquide with a purity higher than 99.999%. Gas flows were regulated with mass flow controllers (Kofloc 8500). The amount

of catalyst used was ca. 0.26 g. Pd and Pd/Ga(x) catalysts were pretreated (heating rate 2 °C/min) at 400 and 500 °C, respectively, in a flow of H_2 (15 NTP cm^3/min) for 2 h. Then, the temperature was lowered to 280 °C, and the catalysts were exposed to a mixture of H_2/CO_2 = 3 (total flow of 20 NTP cm^3/min). Concurrently, the absolute pressure was increased to 800 kPa using a back-pressure regulator (Equilibar). The temperature was decreased consecutively to 260, 240, and 220 °C. The reaction was carried out for 5 h at each temperature. Finally, the temperature was again increased to 280 °C (heating rate 2 °C /min) to verify the stability of the catalysts during the experiment. Reaction products were analyzed online with a gas chromatograph (PerkinElmer Autosystem XL) equipped with a Porapak Q column connected to a thermal conductivity detector followed by a flame ionization detector equipped with a methanizer. The latter allows for more precise quantification of low concentrations of CO and CO_2. The absence of mass and heat transfer limitations at the reaction conditions was demonstrated by calculating adequate criteria [24]. Details about these calculations are in the supplementary material (Section S1). The turnover frequency (TOF) for CO_2 hydrogenation to methanol was based on total external atoms calculated from the average metal particle size measured by XRD. Details on dispersion and TOF calculations are also provided in the supplementary material (Section S2). The approach to equilibrium factor [28] was used to obtain the forward formation rates of CO and methanol from the measured net rates (Section S3).

1.4 DRIFTS experiments

Operando diffuse reflectance infrared Fourier transform spectroscopy (DRIFTS) measurements were performed on a Nicolet 6700 infrared spectrometer (Thermo Scientific) equipped with an MCT detector and a KBr beam splitter. Spectra were obtained by collecting 200 scans with a resolution of 4 cm^{-1}. Experiments were performed using a Smart collector DRIFTS environmental chamber with ZnSe windows. Samples were placed in the cell without packing or dilution. Catalysts recovered after the experiments in the fixed bed reactor were finely ground and loaded onto the sample holder. The gases at the exit of the cell were analyzed by a quadrupole mass spectrometer (Omnistar GSD 320). Once the catalyst (ca. 50 mg) was placed in the cell, it was reduced with H_2 (99.999%, 35 NTP cm^3/min) for 1 h at 300 °C (heating rate 5 °C/min). This procedure ensured the reduction of the surface since used catalysts were briefly exposed to air during loading. After reduction, the cell was cooled to reaction temperature, and the feed was changed to H_2 (21 NTP cm^3/min), CO_2 (7 NTP cm^3/min), and Ar as the internal standard (7 NTP cm^3/min). The reaction was performed at 240 °C for 1 h. The pressure was set at 400 kPa employing an Equilibar back-pressure regulator. The dynamics of surface species was studied by applying rapid changes of concentration using a four-way valve. The CO_2/H_2/Ar standard feed (35 NTP cm^3/min) was rapidly switched to a mixture of H_2 (21 NTP cm^3/min), He (7 NTP cm^3/min), and Ar (7 NTP cm^3/min).This procedure allowed us to follow the concentration of surface species, as well as the relative concentration of methanol in the gas phase, during and after the reaction. DRIFTS analysis of CO adsorption at 30 °C was also carried out. In these tests, the same reduction procedure mentioned above was also applied (a flow of H_2 at 35 NTP cm^3/min at 300 °C for 1 h), and then the cell was cooled to 30 °C under a flow of helium (35 NTP cm^3/min). A flowing mixture of 1% CO/He (40 NTP cm^3/min) was passed through the sample

for 15 min. After that, the cell was purged in a flow of He (35 NTP cm^3/min) during which spectra were collected continuously until only chemisorbed CO was detected.

2. Results and discussion

2.1. Catalytic activity for the hydrogenation of CO_2

Figure 1 shows the forward formation rates of products (CH_3OH and CO) as a function of the Pd/Ga molar ratio of the catalysts. No other products were detected. The results show that Ga addition promotes the rate of methanol formation only in a limited range of Pd/Ga molar ratio. Pd/Ga(0.5) and Pd/Ga(1.0) were the most active catalysts exhibiting methanol formation rates that were one and two orders of magnitude higher than the unpromoted Pd/SiO_2 catalyst (Pd/Ga = ∞). Conversely, methanol formation rates for Pd/Ga(0.2), Pd/Ga(2.0), and Pd/Ga(4.0) were not significantly different when compared to Pd/SiO_2 (Pd/Ga = ∞). These results evidence an absence of a monotonous dependency between the Pd/Ga molar ratio and the methanol formation rate, which would be expected if a synergistic effect was present between Pd and Ga_2O_3 present as separate phases, as proposed by some authors[4]. The highest rates of CO formation were found for Pd and Pd/Ga(4.0) catalysts. Further addition of Ga to Pd for Pd/Ga < 2 leads to a decrease in the rate of CO formation, which is significantly marked at Pd/Ga molar ratios below 1. The different trends observed for the production of methanol and CO as a function of the Pd/Ga molar ratio suggest that Ga has a different influence on the formation of each product. Regarding the stability of the catalysts, the behavior of the formation rates of CH_3OH and CO were studied as a function of time between 220-280 °C indicating that the catalysts were relatively stable as similar activity and selectivity were maintained as observed above (Figure S1).

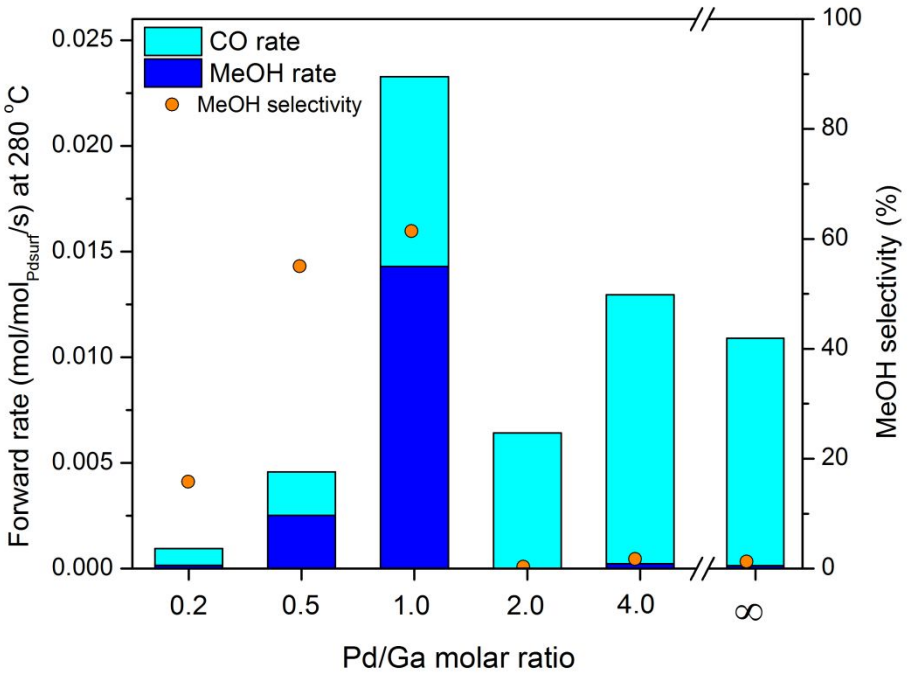

Figure 1. Intrinsic forward rate for the formation of methanol and CO as a function of Pd/Ga molar ratio. H_2/CO_2 = 3, T = 280 °C, P = 800 kPa, SV = 80 cm^3 reactants/g_{cat}/min.

Figure 2 shows the variation of the apparent activation energies with respect to the Pd/Ga molar ratio (Arrhenius plots are shown in Figure S2). CO_2 conversions were low in each sample in the analyzed temperature range, which justified the calculation of the E_{app} at differential conditions (Table S2). In addition, we considered for the calculation of E_{app} that CO and CH_3OH are formed in parallel, as it has been shown in previous works [18, 29]. A decrease in apparent activation energy for methanol formation was observed with the increasing amount of Ga in the catalysts (65 to 47 kJ/mol). This suggests that the presence of Ga either may be generating a difference in the nature of the sites or changing the reaction pathway for methanol formation. The apparent activation energy is related to the activation energy of the kinetically relevant step of the mechanism and to the adsorption enthalpies of reactants and most abundant surface intermediates[30]. Consequently, variations in E_{app} could be related to a change in these parameters, which are related to the interaction of adsorbates with the surface. Interestingly, the variations in activation energy are verified for methanol formation but not significantly for CO formation (E_{app} 75-79 kJ/mol). We will further elaborate on that in a later section.

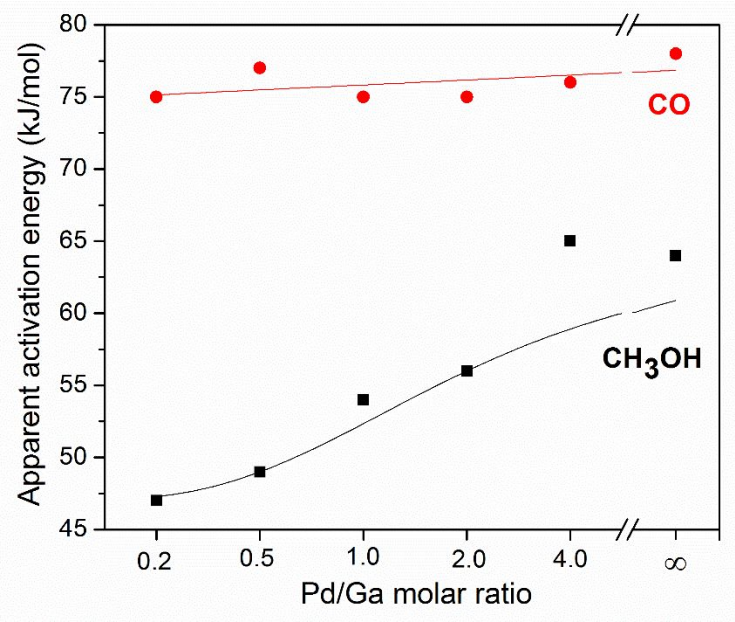

Figure 2. Apparent activation energies for CH_3OH and CO formation with respect to the Pd/Ga molar ratio. H_2/CO_2 = 3, P = 800 kPa, T = 220-280 °C. Lines were added to guide the eye.

The E_{app} values for methanol and CO formation coincide with previous reports [12, 17, 18], which show E_{app} values between 59 and 72 kJ/mol for methanol formation and between 82 and 94 kJ/mol for CO formation over Pd and bimetallic Pd-Ga. The systematically higher E_{app} values for CO formation imply that methanol selectivity is favored at lower temperatures (Figure S3). Our reported intrinsic forward formation rates of methanol are of the same order as those reported by Ota et al. using a PdMgGa catalyst (H_2/CO_2 = 3, P = 3 MPa, T= 250 °C, SV = 250 cm^3 reactants/g_{cat}/min) [17]. Indeed, if the rates in the present work are corrected for temperature with the obtained E_{app} and assuming a 1.5-order dependence on total pressure [1, 31] the resulting methanol formation total rates for Pd/Ga(0.5) (1.8×10^{-3} $mol_{methanol}/mol_{Pdsurf}/s$) and Pd/Ga(1.0) ($5.8\times10^{-3}$ $mol_{methanol}/mol_{Pdsurf}/s$) would be similar to the values reported for the PdMgGa catalyst (2.5×10^{-3} $mol_{methanol}/mol_{Pdsurf}/s$). Additionally, the forward formation rates of CO obtained here are of the same order of magnitude as those reported for the PdMgGa catalyst (~4×10^{-3} s^{-1}), except for the cases of the samples with the highest amounts of Ga, that is, Pd/Ga(0.5) and Pd/Ga(0.2), for which the activity to CO was lower.

From the above catalytic activity results and information reported in the literature, it is difficult to unambiguously define the role of Ga as a promoter of Pd in CO_2 hydrogenation to methanol. In the case of a synergistic effect between separate phases of Pd and Ga_2O_3, an increase in the rate of formation of methanol would be expected with addition of Ga (i.e., decreasing Pd/Ga molar ratio), which did not occur. These results highlight the necessity of a systematic and detailed catalyst characterization to gain more insights on the effect of Ga as a promoter in Pd catalysts for the hydrogenation of CO_2 to methanol.

2.2 Catalysts characterization

Figure 3 shows TEM images and the corresponding particle size distributions for the six evaluated catalysts (more images are found in the supplementary information, Figure S4). With the exception of Pd/Ga(0.2), which exhibited an average particle size of 27 nm, the synthesis method led to minimum variations in the average particle diameters among the studied samples (~8-15 nm). This will facilitate a more rigorous comparison of the activity and selectivity of the formed metallic phases given the reported structure sensitivity of the reactions under study [18, 32].

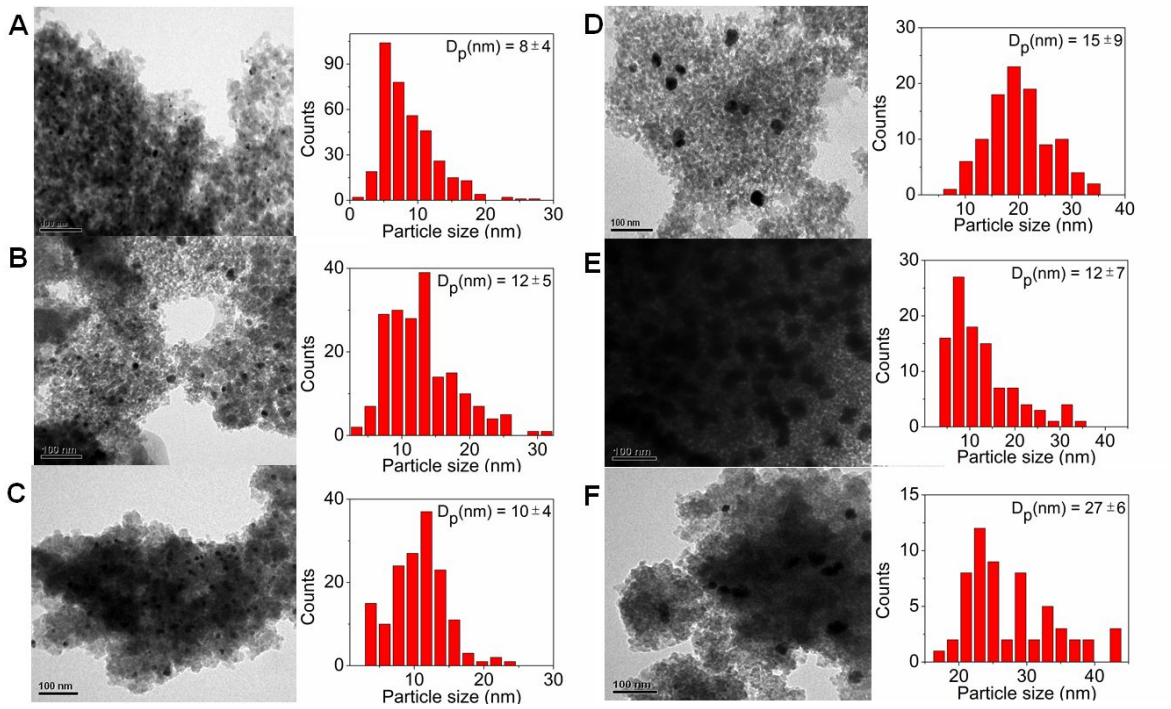

Figure 3. Transmission electron microscopy images and their corresponding particle size distribution, average particle size (Dp), and standard deviation for (A) Pd, (B) Pd/Ga(4.0), (C) Pd/Ga(2.0), (D) Pd/Ga(1.0), (E) Pd/Ga(0.5), and (F) Pd/Ga(0.2) catalysts. The bar in the images represents 100 nm.

Figure 4 displays the XRD patterns of the catalyst samples under study after reaction tests. All samples showed the presence of Pd-based crystalline phases. In the case of Pd and all Ga promoted catalysts with relatively low Ga content or high Pd/Ga molar ratios (Pd/Ga(2.0) and Pd/Ga(4.0)), only intense signals due to metallic palladium crystals were observed at 2θ = 40.0 and 46.4°. In the case higher Ga content such as in Pd/Ga(1.0), strong signals due to an intermetallic Pd_2Ga phase were found at 39.8, 41.3, 44.6, and 48.2°. For samples with a higher amount of Ga (i.e., Pd/Ga(0.2) and Pd/Ga(0.5)) the exact crystalline phase formed could not be identified with the available databases, nevertheless, a bimetallic Pd-Ga phase is likely present since monometallic Pd and Ga compounds were not observed. It is important to highlight that a pure Pd phase and crystalline gallium oxide (Ga_2O_3) were not detected in samples with an excess of Ga (Pd/Ga(0.2), Pd/Ga(0.5), and Pd/Ga(1.0)).

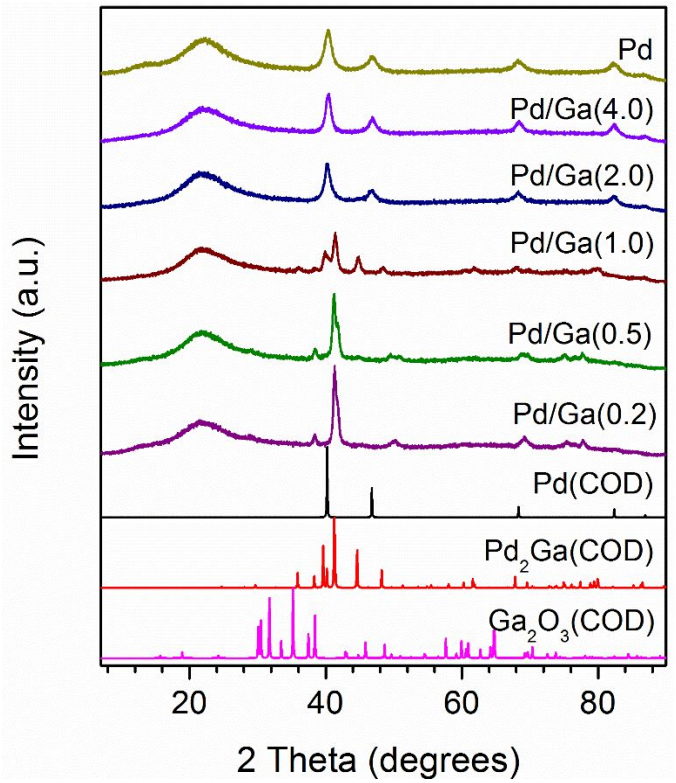

Figure 4. XRD results of Pd-Ga catalyst samples recovered after reaction tests. Standards from the COD database[25]: Pd (1011105) and Pd_2Ga (8102983) and β-Ga_2O_3 (2004987). (http://www.crystallography.net/cod/).

Table 1 summarizes the estimates of the average particle sizes for the metallic domain (e.g., Pd, Pd-Ga bimetallic phases) in the supported catalysts after reaction. In Pd, Pd/Ga(4.0), Pd/Ga(2.0), Pd/Ga(1.0), and Pd/Ga(0.5) catalysts the average particle sizes obtained by TEM and XRD show a clear agreement. For monometallic Pd catalyst, the particle size estimated by oxygen chemisorption (9 nm) also agreed with TEM and XRD data. The significant difference between TEM and XRD particle size observed for Pd/Ga(0.2) is probably due to the fact that in this sample there are Ga_2O_3 polycrystalline aggregates that prevent the correct resolution of Pd particles, hence overestimating their size. Because of peaks overlap, the most intense peaks of the XRD patterns in the catalysts with the highest Ga content and thus the lowest Pd/Ga molar ratio (0.5 and 0.2) were subjected to a deconvolution to allow a safe use of the Scherrer equation (Figure S5). We also calculated the surface and volume-weighted average diameter from the TEM particle size distribution[24] (Table S3). The resulting values are larger than the number-average particle sizes presented in Table 1. Nevertheless, the differences among the samples are of the same order. Consequently, the similarity of the results among the different estimation methods confirmed that the sizes of the metallic particles for the different catalysts reported in Table 1 did not vary significantly, which minimizes the effect due to particle size on the formation rates of methanol in the catalysts promoted by Ga with respect to the rates for the unpromoted Pd catalyst. It has been shown that intrinsic methanol and CO formation rates do not vary significantly for this reaction in the 9-20 nm range of particle sizes [18, 33, 34].

Table 1. Average particle size of Pd metal determined by TEM, XRD, and O_2 chemisorption and corresponding metal dispersion for Pd and Pd-Ga catalysts.

Sample	Dp_{TEM} (nm)[a]	Dp_{XRD} (nm)[b]	Dp_{Chem} (nm)[c]	Metal dispersion (%)[d]
Pd[c] (Pd/Ga(∞))	8±4	9	9	12
Pd/Ga(4.0)	12±5	13	-[e]	9
Pd/Ga(2.0)	10±4	9	-[e]	12
Pd/Ga(1.0)	15±9	15	-[e]	8
Pd/Ga(0.5)	12±7	13	-[e]	9
Pd/Ga(0.2)	27±6	18	-[e]	6

[a] Determined by TEM.

[b] Determined by X-ray diffraction.

[c] Determined from Oxygen chemisorption.

[d] Dispersion based on XRD results

[e] Due to unknown chemisorption stoichiometry, this technique was not used for quantifying the dispersion of catalysts containing Ga.

TEM-EDS characterization in Figure 5 shows that for Pd/Ga(1.0), Pd/Ga(0.5), and Pd/Ga(0.2), Pd and Ga are spatially distributed in the same positions suggesting that the majority of the metal particles are intimately mixed likely forming solid solutions of intermetallic nature. A linear EDS atom scan analysis performed for the Pd/Ga(0.2) (Figure S6) showed that Pd and Ga distribution followed similar trends confirming the presence of a homogeneous metal mixture. This, however, was not the case for Pd/Ga(4.0) and Pd/Ga(2.0) where Pd is most likely forming a monometallic phase in agreement with XRD results. Slight variations in Ga distribution with respect to Pd probably indicate the presence of a different Ga phase (e.g., Ga_2O_3). Additional EDS mappings are shown in Figure S7.

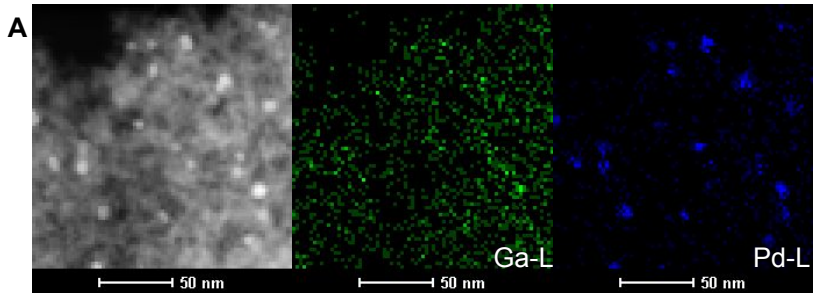

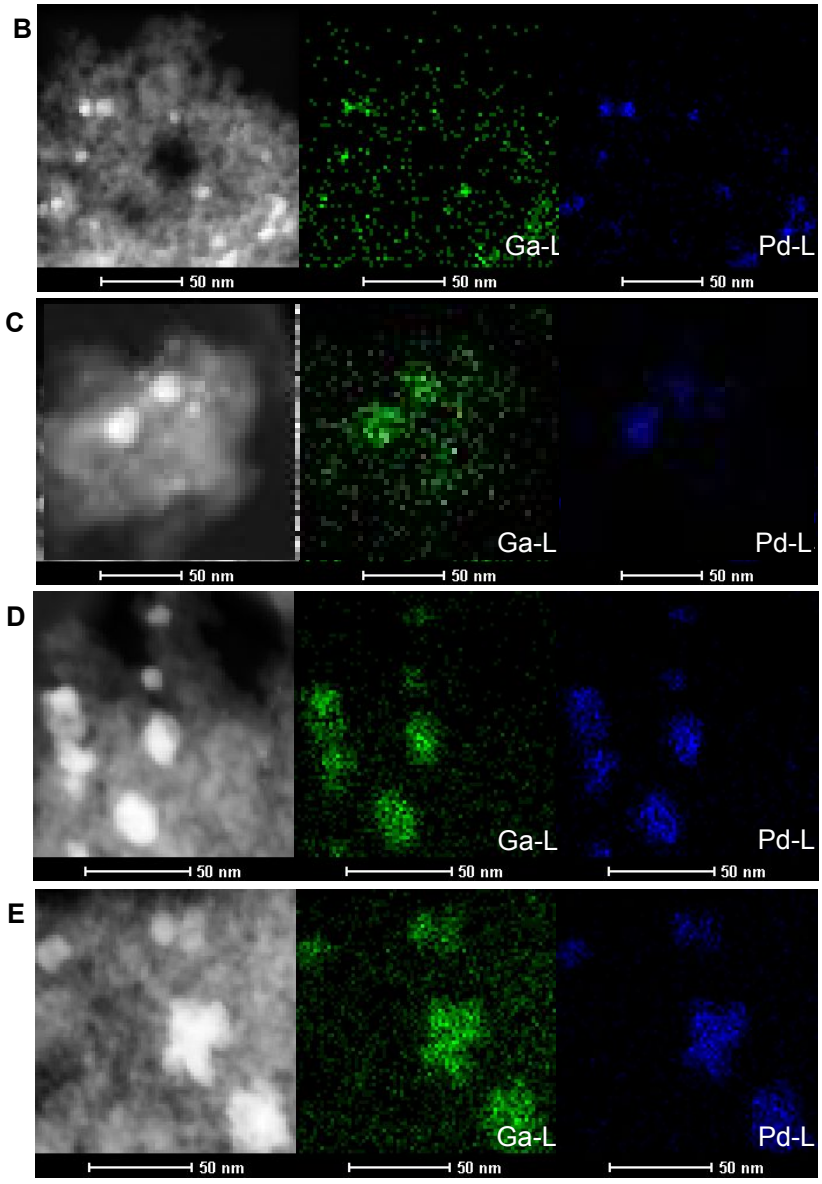

Figure 5. TEM-EDS characterization of the corresponding spatial distribution of Pd and Ga in: (A) Pd/Ga(4.0), (B) Pd/Ga(2.0), (C) Pd/Ga(1.0), (D) Pd/Ga(0.5) and Pd/Ga(0.2) catalysts. The bar in the images corresponds to 50 nm.

2.3 Infrared analysis of CO adsorption

DRIFTS analysis of adsorbed CO was used to investigate the surface properties of the catalysts after in situ reduction in a flow of H_2 at 300 °C. Figure 6 shows IR spectra of chemisorbed CO at 30 °C which is characteristic of CO adsorbed on different configurations on metal surfaces. For example, the IR absorption bands observed in the 2100-2000 cm^{-1} range correspond to linearly adsorbed CO on Pd^0, whereas the bands at 1980-1800 cm^{-1} indicate 2- and 3-fold bridged CO on Pd^0 [35].

For the monometallic Pd catalyst the strongest IR absorption bands were observed at 1978 and 1934 cm^{-1}. These bands correspond to CO adsorbed through multiple bonds on Pd^0 and are typical of adsorption on monometallic surfaces as well as characteristic of catalysts with surface atoms of Pd with a high degree of coordination (large particles) [36]. Also, a less intense band at 2084 cm^{-1} was observed, which is related to CO linearly adsorbed on Pd [36]. Since the surface of this catalyst is dominated by a monometallic phase of Pd, then the observed large particle sizes characterized by relatively higher coordinated atoms would allow CO to be absorbed in different Pd surface positions.

When low amounts of Ga are added, as in Pd/Ga(4.0) and Pd/Ga(2.0) catalysts, a clear decrease in the intensity was observed for the bands corresponding to CO adsorbed on multiple Pd sites (1980-1972 cm^{-1}) relative to CO linearly adsorbed on isolated Pd (2084 cm^{-1}). The changes to both CO adsorption bands are assigned to Ga preferential occupation of Pd hollow sites which not only decreased the number of Pd multi-sites density but also increased that of isolated Pd. Because of the absence of Pd-Ga intermetallic phases on the samples as evidenced from XRD, such Ga location should result more in a geometric than an electronic effect. This geometric effect was also observed by Jbir et al. [2], who reported that promotion of Pd with Sn caused the suppression of Pd^0 sites that favored CO adsorption via Pd-Pd bridge or multiple sites.

At a higher Ga loading (Pd/Ga(1.0)) the bands related to CO adsorbed through multiple Pd bonds disappeared while weak bands due to linearly adsorbed CO (2100 and 2150 cm^{-1}) evolved, thus, indicating that Ga addition promoted the formation of Pd sites that are somewhat isolated. A similar observation was reported by Kovnir et al. [37], who studied the semi-hydrogenation reaction of acetylene on Pd-Ga catalysts, and which was attributed to the presence of fully isolated Pd atoms on intermetallic Pd-Ga surfaces. This observation is consistent with our XRD results shown above, where a crystalline Pd_2Ga phase was identified for Pd/Ga(1.0). Similar to Pd/Ga(1.0), the IR spectrum for Pd/Ga(0.5) is characterized by the presence of a peak at 2092 cm^{-1} and by the absence of the peak associated with Pd-Pd bridge and multi-sites CO adsorption as a result of the formation of intermetallic phases. Finally, for Pd/Ga(0.2), the catalyst with the highest Ga content, CO adsorption was negligible despite the presence of an intermetallic phase (XRD), suggesting that the surface availability of Pd in the Pd-Ga phase was very low due to covering by Ga_2O_3 oxide (observed by TEM-EDS).

Overall, Figure 6 shows a decrease in the amount of linearly adsorbed CO in the catalysts containing higher amounts of Ga (i.e., Pd/Ga(1.0), Pd/Ga(0.5), and Pd/Ga(0.2)) compared to those with lower Ga content: Pd, Pd/Ga(4.0), and Pd/Ga(2.0). This can be related to the coating of metallic phases by Ga_2O_3 layers which would limit the availability of surface palladium sites [4, 38]. The latter is also consistent with the decrease in the rates of formation of methanol for Pd/Ga(0.5) and Pd/Ga(0.2) compared to Pd/Ga(1.0) as shown in Figure 1. The above analysis indicates that the activity towards methanol formation correlates more strongly with the site type (bimetallic *vs.* monometallic) than with a synergistic effect between the metallic and oxide phases. The coexistence of Ga oxides with PdGa intermetallic compounds in the best catalysts does not allow us to discard a synergistic effect between

those phases as a cause for their high activity. However, in the case of catalysts with low amount of Ga, the coexistence of Pd and Ga_2O_3 phases does not lead to active catalysts.

Another interesting aspect evidenced in Figure 6 is the significant displacement observed for the peaks corresponding to the linear adsorption of CO for Pd/Ga(1.0) and Pd/Ga(0.5) (2150-2092 cm^{-1}) with respect to the CO adsorption bands in Pd/Ga(4.0) and Pd/Ga(2.0) (2085 cm^{-1}). A similar behavior was reported by Zorn et al. [36] for Pd catalysts that suffer a variation in their oxidation state ($Pd^{\delta+}$) thus generating a change in the electronic structure of the active sites, which lowered their CO adsorption energy (~0.8 eV). This result is also consistent with the formation of a new intermetallic crystalline phase via covalent interaction between Pd and Ga as reported by Wowsnick et al. [38]. The existence of two bands (2100 and 2150 cm^{-1}) may imply that there is a heterogeneity of CO adsorbing Pd sites [2].

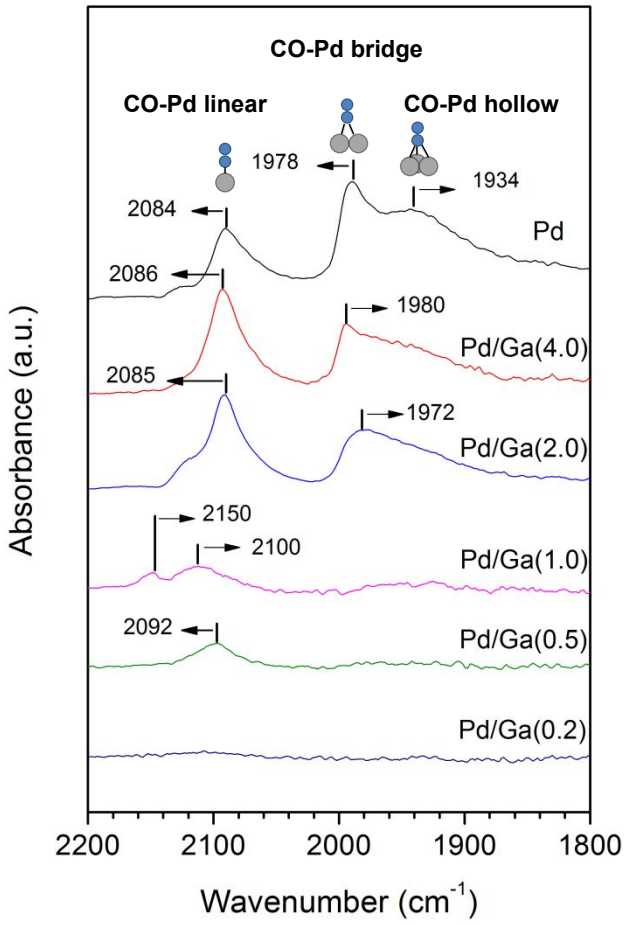

Figure 6. CO adsorption at 30 °C analyzed by DRIFTS on Pd-Ga catalysts as a function of their Pd/Ga ratio. Prior to measurements, catalysts were reduced in situ in H_2 at 300 °C.

2.4 Quasi in situ XPS

The Pd-Ga catalysts were also characterized by Quasi in situ XPS after applying different treatments in the High-Pressure Cell of the instrument which included: (i) reduction in H_2 for 1 h at 500 °C and 101 kPa, (ii) reduction in H_2 for 1 h at 500 °C and then oxidation in O_2 for 1 h at 25 °C and 101 kPa, and (iii) reduction in H_2 for 1 h at 500 °C and 101 kPa and then reaction conditions in a flow of H_2/CO_2 = 3 for 1 h at 260 °C and 101 kPa. This pressure is lower compared to the fixed bed reactor (800 kPa) because of technical limitations. Nevertheless, we think that this still permits to obtain meaningful comparisons among the different catalysts.

Figure 7 shows the Pd 3d and Ga 2p spectra for all catalysts after the reduction pretreatment at 500°C. For Pd/Ga(4.0) and Pd/Ga(2.0) catalysts the binding energy (BE) for the Pd $3d_{5/2}$ core level was 335.1 eV (Figure 7A) indicating that Pd is in the metallic state (Pd^0) [37, 39]. For the case of Pd/Ga(1.0) and Pd/Ga(0.5), the Pd $3d_{5/2}$ BE shifted to higher values (335.7 and 336.0 eV, respectively) suggesting that Pd augmented its oxidation state. Some authors have claimed that this shift is due to the formation of an intermetallic Pd-Ga phase [37, 39]. Such an interpretation is consistent with XRD, TEM-EDS, and CO-IR evidence shown above. Precedent works that applied similar calcination and reduction procedures have also detected bimetallic PdGa but not mixed Pd-Ga-O oxides[40, 41]. For Pd/Ga(0.2), the BE corresponding to the Pd $3d_{5/2}$ electrons were more difficult to resolve due to the small concentration of surface palladium (atomic concentration < 0.01%), which is consistent with Figure 6 indicating a lack of surface metallic Pd sites, likely due to coating with Ga_2O_3. Figure 7B shows the Ga 2p spectra after the same reducing conditions. The catalysts with the higher amount of Ga, Pd/Ga(0.2) shows a Ga $2p_{3/2}$ peak at 1120.6 eV. This BE could be associated to Ga_2O_3, however it is somewhat at higher values compared to the normally reported[42]. The higher values reported here could be due to differential charging linked to the heterogeneity of the samples. However, the kind of differential charging that we may have experienced during our analyses does not lead to peak deformation hence not harming chemical surface analysis. On the other hand, other researchers have reported BEs of the same order as the ones we found, for thin films of gallium oxide made over glass substrates[43]. In addition, Hou et al. reported a BE of 1119.7 eV for Ga^{3+} oxides[44].

Catalysts with decreasing Ga content such as Pd/Ga(0.5) and Pd/Ga(1.0) present this peak at lower BE (at 1120.2 eV and 1119.6 eV respectively), indicating a more reduced state of Ga atoms, which is consistent with an increase in the concentration of intermetallic Pd-Ga at the surface, due to a lower coverage with Ga oxide. The detection of Ga oxides is an indication that there is a Ga surplus that is not incorporated into the intermetallic compounds.

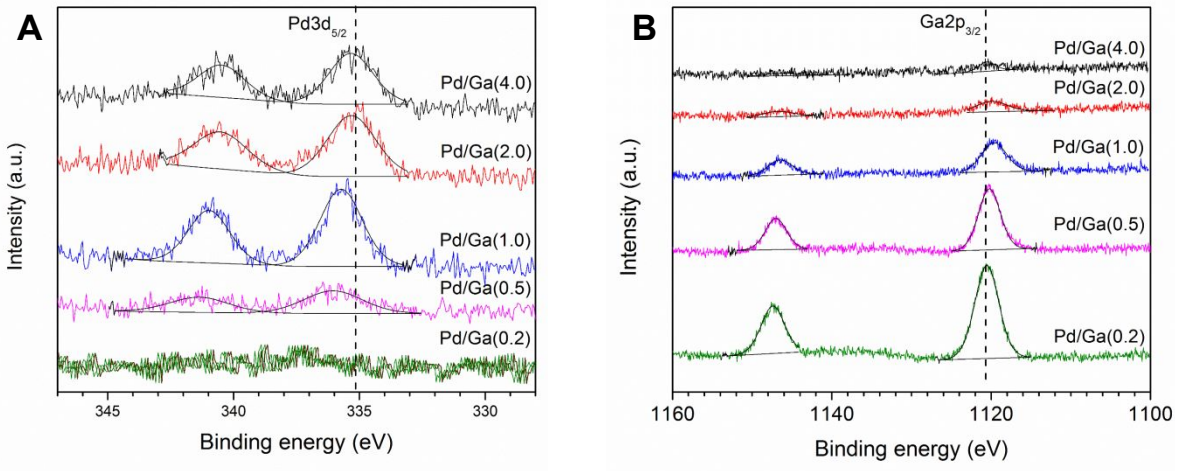

Figure 7. Pd-Ga catalysts quasi in situ XPS results: (A) Pd 3d and (B) Ga 2p after treatment in H_2 at 500 °C for 1 h in the high-pressure cell of the XPS platform.

Figure 8 shows the Pd 3d spectra for all catalysts after they were submitted to the different pretreatments. The XPS results for low Ga content samples, Pd/Ga(4.0) and Pd/Ga(2.0) (Figures 8A and 8B), exposed to oxidation conditions show Pd $3d_{5/2}$ BEs at 335.8 eV, which can be assigned to Pd^{+2} in PdO [45, 46]. When these catalysts were exposed to reduction conditions, this signal shifted towards a lower BE of 335.1 eV due to the formation of Pd^0. At reaction conditions, the BEs were 335.2 eV, confirming the predominance of Pd monometallic phase at CO_2 hydrogenation conditions. On the contrary, the Pd $3d_{5/2}$ BEs for Pd/Ga(1.0) and Pd/Ga(0.5) remained fairly unchanged (e.g., 335.8 and 336.0 eV, respectively, after reduction) regardless of the nature of the pretreatment gas (Figures 8C and 8D). In the case of Pd/Ga(0.2), this analysis was not possible due to the to the low concentration of palladium on the surface. XPS results confirm that the catalyst surface in samples with Pd/Ga < 1.0 is characterized by the presence of intermetallic phases at reaction conditions.

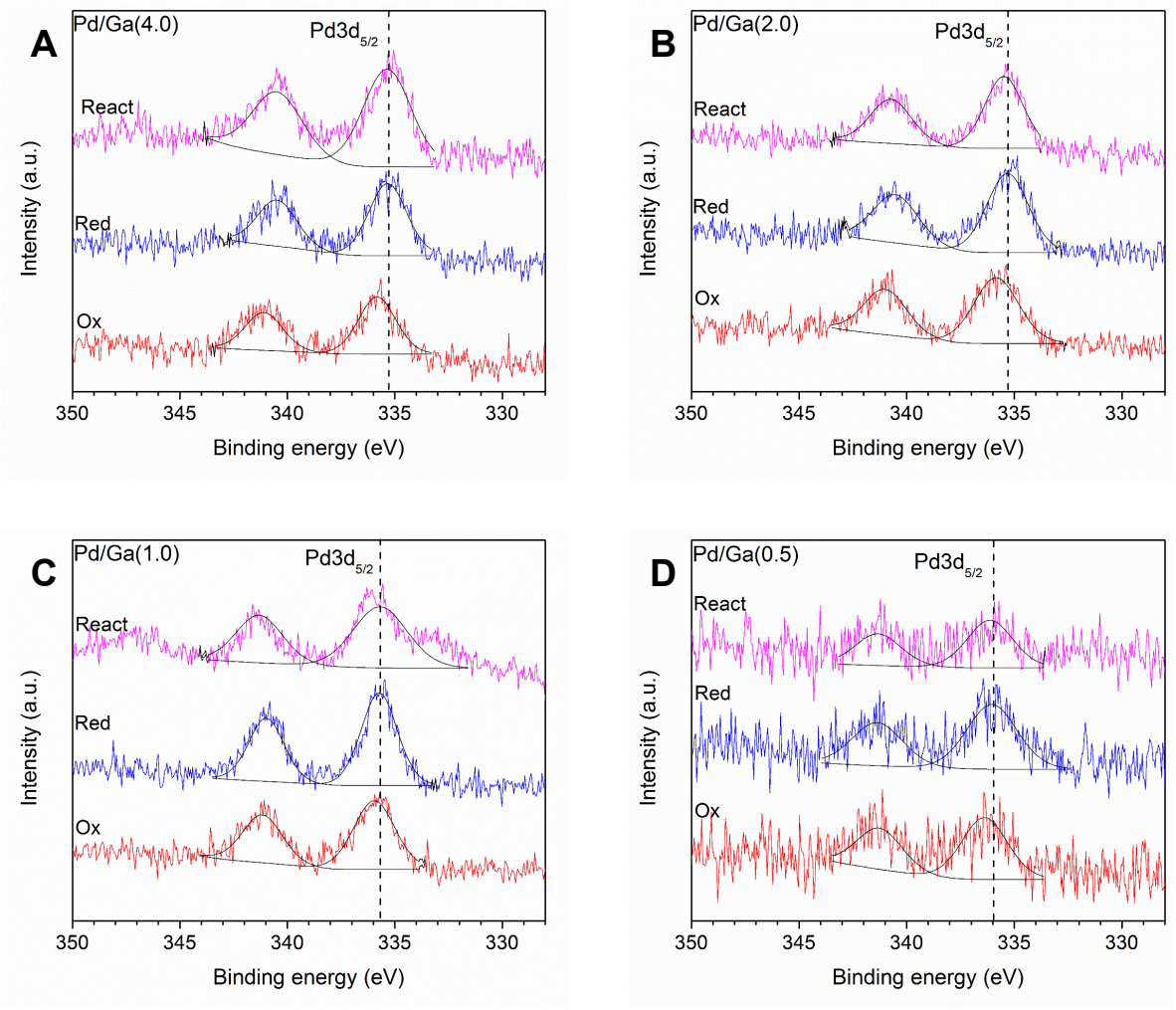

Figure 8. Quasi in situ XPS results for Pd 3d region for (A) Pd/Ga(4.0), (B) Pd/Ga(2.0), (C) Pd/Ga(1.0) and (D) Pd/Ga(0.5) catalysts after different gas treatments. (Ox) oxygen flow (20 NTP cm^3/min, 101 kPa) at 25 °C; (Red) hydrogen flow (50 NTP cm^3/min, 101 kPa) at 500 °C; (React) reaction conditions at 260 °C (40 NTP cm^3/min, H_2/CO_2 = 3, 101 kPa).

Figure S8 (in the supplementary information) summarizes the Pd $3d_{5/2}$ BEs for all catalysts as a function of the Pd/Ga molar ratio. The Pd $3d_{5/2}$ BE position suffered less variation under the applied pretreatments for Pd/Ga(1.0) and Pd/Ga (0.5) when compared to Pd/Ga(2.0) and Pd/Ga(4.0). This structural stability in the Pd/Ga(1.0) and Pd/Ga (0.5) catalyst samples appear to be related to strong covalent interactions between Pd and Ga due to the formation of Pd-Ga intermetallic phase as proposed by Wowsnick et al. [38].

Similar to Figure 8, Figure S9 shows the Ga $2p_{3/2}$ XPS spectra for all catalysts also treated at different conditions. The Ga $2p_{3/2}$ BE for Pd/Ga(4.0) and Pd/Ga(2.0) were unaltered after the reduction pretreatments, with BEs higher than 1120.0 eV, confirming the stability of the Ga oxidized phase on the catalyst surface. Such Ga $2p_{3/2}$ BE behavior confirmed that the shifts in Pd $3d_{5/2}$ BEs were primarily due to the formation of a Pd^0 phase rather than the presence of an intermetallic phase. In the case of Pd/Ga(1.0) and Pd/Ga(0.5), a decrease

in Ga $2p_{3/2}$ BEs of 0.4 and 0.2 eV, respectively, was evidenced. This trend is consistent with Ga $2p_{3/2}$ results on similar Pd-Ga catalysts by Osswald et al. [47], who also evidenced the formation of a bimetallic Pd-Ga phase and found a decrease in BEs after a hydrogen treatment at 400 °C. It is important to note that in all samples under the different treatments applied, the presence of surface Ga_2O_3 was identified, but only where bimetallic Pd-Ga phases were detected (XRD, XPS and CO-IR), a significant improvement in the activity towards methanol formation with respect to Pd/SiO_2 was evidenced.

Figure S10 shows the ratio between palladium (Pd/(Si + Ga + Pd)) and Ga (Ga/(Si + Ga + Pd)) surface concentrations measured by XPS with respect to the corresponding nominal concentrations. The consistently higher relative Ga concentration compared to Pd suggests that Ga is better dispersed on the surface. Additionally, the calculated relative Pd ratio for high Ga containing samples, Pd/Ga(0.5) and Pd/Ga(0.2), decreased to a greater extent (0.05 and <<0.05) with respect to the nominal values when compared to the other analyzed samples (~0.08). These results suggest that Ga prevails on the catalyst surface and that its excess affects the availability of Pd sites. A decrease in surface Pd site density with an increase in Ga content is probably due to the formation of an oxidized Ga phase which is more marked for Pd/Ga(0.5) and quite significant for Pd/Ga(0.2) where Pd surface content was quite low and below the detection limit of the technique employed. Furthermore, the variations between the Pd/(Si + Ga + Pd) measured by XPS under reduction conditions (Figure S10) were not as significant as the differences in activity towards the formation of methanol. For example, the measured Pd relative concentrations varied less than one fold (~0.05-0.08), whereas the catalytic activity for Pd/Ga(1.0) and Pd/Ga(0.5) were one and two orders of magnitude, respectively, higher than that for Pd, Pd/Ga(4.0) and Pd/Ga(2.0) catalysts. These results demonstrate that the difference in activity towards methanol formation on Pd in Pd/Ga(1.0) and Pd/Ga(0.5) compared to Pd, Pd/Ga(4.0) and Pd/Ga(2.0) is due to the presence of active sites of different nature, namely, intermetallic Pd-Ga *vs.* Pd sites, respectively. However, it is important to note that these results do not rule out a synergistic effect between bimetallic Pd-Ga and Ga_2O_3 as proposed by Snider et al[14] in the case of Pd-In and In_2O_3.

2.5 Operando DRIFTS

Figure 9A shows the operando DRIFTS results for all catalysts under reaction conditions (H_2/CO_2 = 3, T = 240 °C and P = 400 kPa) in the 2750-3000 cm^{-1} wavenumber range. Three main bands were detected: 2852-2856, 2907-2931, and 2960 cm^{-1}. The first two bands, 2852-2856 and 2907-2931 cm^{-1}, are similar in frequencies to adsorption doublets found after dosing formic acid on promoted palladium catalysts. The former band is related to the υ_s (CH) stretching vibration, while the latter corresponds to the υ_{as} (OCO) + δ (CH) combination bands [48, 49]. These vibrations indicate the existence of bidentate formate species (b-HCOO) on the catalyst surface at reaction conditions. It is important to note that this adsorption has been reported to occur on Pd sites and not on Ga sites in their oxidized form [48, 49]. These bands were detected on all of the Pd-Ga and Pd catalysts, except on Pd/Ga(2.0) and Pd/Ga(0.2). For the latter, it was demonstrated in previous sections that gallium oxide affected the availability of surface palladium sites. A third band centered at 2960 cm^{-1} was

also observed when adsorbed formate was also present, which was ascribed to υ_{as} (CH) of methoxy species. This is consistent with a CO_2 hydrogenation mechanism towards methanol formation occurring via the reduction of b-HCOO [1, 13, 18]. Although some of the marked bands are weak, they are clearly distinguished when comparing with blank spectra and their evolution is noticeable during dynamic experiments (Figure S11).

Figure 9B shows the methanol mass spectrometer signal (m/z = 31) at the exit of the DRIFTS cell under reaction conditions. These results resemble those in Figure 1 corresponding to fixed bed reactor methanol formation rates for all catalyst samples. Interestingly, Pd and Pd/Ga(4.0) present low activity towards methanol formation (Figure 9B). However, both catalysts show the presence of bidentate formate and methoxy species on the catalyst surface (Figure 9A). To assess the reactivity of the observed surface species additional experiments were carried out by switching from reaction conditions to a flow of H_2 (21 NTP cm^3/min, 400 kPa). For Pd and Pd/Ga(4.0), formate and methoxy species remained on the catalyst surface even after 1 h of contact with H_2 after reaction (Figure S11). This indicates that, on these samples, the reduction of formate species is carried out slowly probably causing a lower intrinsic rate towards methanol formation. Conversely, for catalysts containing bimetallic Pd-Ga phases; namely, Pd/Ga(1.0) and Pd/Ga(0.5), formate and methoxy peaks were observed under reaction conditions but disappeared completely after H_2 flow. Therefore, these surface formate species adsorb less strongly on Pd/Ga(1.0) and Pd/Ga(0.5) than on Pd and Pd/Ga(4.0). A direct consequence of this change is that formate species are reduced at a higher rate resulting in higher methanol formation rates as we found for Pd/Ga(1.0) and Pd/Ga(0.5) catalysts, which would be expected if b-HCOO acts as an intermediate and not as spectator species.

For the samples containing bimetallic phases (Figure 9A), Pd/Ga(1.0) and Pd/Ga(0.5), the peak corresponding to υ_{as} (OCO) + δ (CH) appears at lower wavenumber (2907 cm^{-1}) when compared to Pd and Pd/Ga(4.0) catalysts (~2930 cm^{-1}), but without significant changes in the υ_s (CH) peak band position (~2854 cm^{-1}). The difference in the position of the υ_{as} (OCO) peak probably arises from changes in electronic density between Pd-Ga *vs*. Pd surfaces which modifies the adsorption strength of formate species as also evidenced from the reactivity of formate species (Figure S11). As the bidentate formate is adsorbed through its O atoms, it is expected that changes in the υ_{as} (OCO) vibrations will be more marked than compared to the C-H bond (i.e., υ_s (CH)).

Finally, Pd/Ga(2.0) and Pd/Ga(0.2) samples showed the lowest activities towards methanol formation (Figures 1 and 9B), which is consistent with the operando DRIFTS results in Figure 9A, where bands due to adsorbed species were not detected at the sensitivity level of the IR spectrometer. The correlation between surface formate and methoxy species shown in Figure 9A with respect to the degree of catalytic activity at the studied reaction conditions is evident. Therefore, at the present conditions, formate species are likely to be reaction intermediates in the methanol formation mechanism as suggested by prior works [1, 13, 18]. On Pd catalysts promoted with Cu, Jiang et al. [48] observed a correlation between the intensities of formate adsorption bands and higher methanol formation rates, attributing it to a greater surface coverage of b-HCOO. In the present work, intense bands corresponding to adsorbed

b-HCOO on Pd and Pd/Ga(4.0) catalysts were observed, confirming that the surface in these samples predominantly consists of a Pd metallic phase. However, due to the monometallic nature of these Pd sites, the hydrogenation process of formate to methoxy species is slower than on the surface of bimetallic phases. Previous works that studied this reaction with infrared spectroscopy proposed that b-HCOO is an intermediate species in a limiting reaction step, thus defining the net rate towards methanol formation from CO_2 hydrogenation [1, 13, 48-50]. It is important to highlight that some authors[4] have reported the adsorption of formate species in Ga_2O_3 through the presence of bands between the wavenumber of 1200 and 2200 cm^{-1}. However, in this work it was not possible to analyze, due to an excess of noise in that area, but our results show that the adsorption of formate species occurs in the metallic sites of Pd (as it was evident in Pd/SiO_2) as observed by other authors[48].

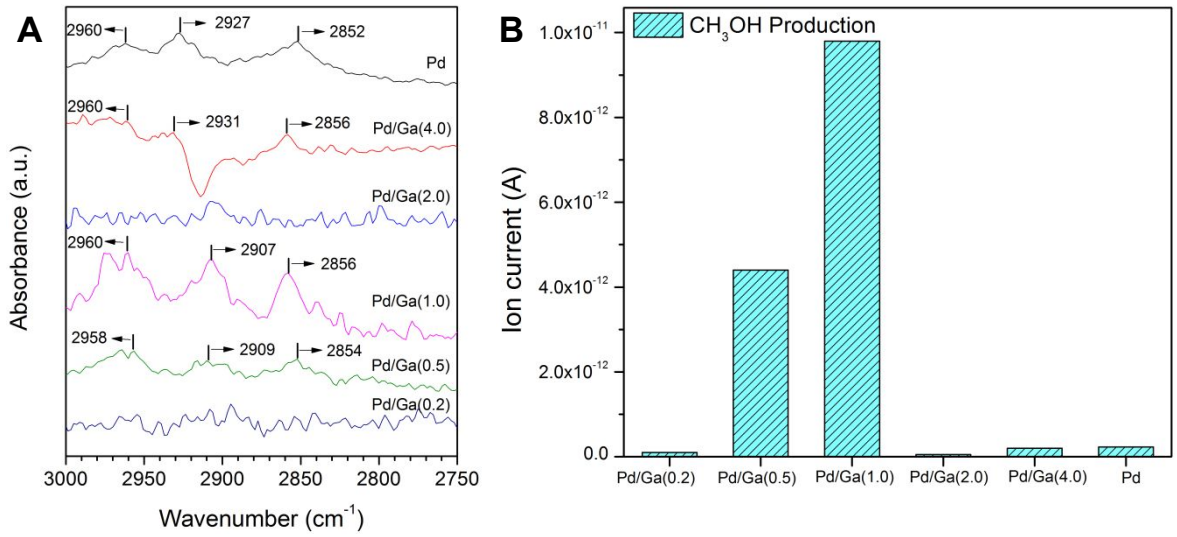

Figure 9. (A) Operando DRIFTS results for all catalysts and the corresponding (B) analysis of methanol production by mass spectrometry (m/z = 31) during the hydrogenation of CO_2 at steady state. Reaction conditions: T = 240 °C, P = 400 kPa, H_2/CO_2 = 3.

Figure 10 shows the operando DRIFTS spectra in the wavenumber range corresponding to the different forms of adsorbed CO detected at reaction conditions (T = 240 °C, P = 400 kPa, H_2/CO_2 = 3). Pd, Pd/Ga(4.0), and Pd/Ga(2.0) catalysts show the most intense peaks at 1930-1955 cm^{-1} corresponding to the bridge and hollow adsorption of CO when compared to linear CO adsorption. This is consistent with Figure 6 (probing CO adsorption at 30 °C) where it was concluded that the surface of these samples was enriched by the monometallic Pd phase. For these samples, this shows that there is a Pd monometallic phase at reaction conditions which is responsible for the adsorption of bidentate formates. From Figure 10, a decrease in the intensity of the peaks associated with the linear and multiple adsorption of CO on Pd was also noted with increasing Ga amount for Pd, Pd/Ga(4.0), and Pd/Ga(2.0). As mentioned earlier, this behavior should be caused by the covering of Pd with excess Ga present as an oxidized phase. This is consistent with the hypothesis that methanol formation depends on the availability of Pd metallic sites on the catalyst surface, which are responsible

for formate species adsorption, as clearly evidenced for Pd/Ga(2.0), the least active catalyst among Pd, Pd/Ga(4.0), and Pd/Ga(2.0) group. In the case of Pd/Ga(1.0), Pd/Ga(0.5), and Pd/Ga(0.2), only linearly adsorbed CO was primarily observed with negligible bridged and hollow adsorbed CO, which is characteristic of a surface populated by bimetallic Pd-Ga phases. For these samples, this behavior is similar to the one shown in Figure 6, which also confirms the presence of these phases. Another similar behavior with respect to Figure 6 is the displacement to higher wavenumber of the bands corresponding to the linear adsorption of CO on Pd/Ga(1.0), Pd/Ga(0.5), and Pd/Ga(0.2) confirming the different nature of these sites at these reaction conditions. Additionally, the decrease in the availability of surface Pd-Ga bimetallic sites with the increase in Ga amount was also noticeable. For example, on Pd/Ga(0.2), linearly adsorbed CO was barely detected, which explains the absence of adsorption bands for formate and methoxy species in Figure 9. This analysis further confirms that Pd or Pd-Ga sites are responsible for adsorption of formate species and that their monometallic or bimetallic nature defines the magnitude of the reaction rate towards methanol formation. The formation of CO can be followed by looking at the gas phase CO peak appearing at 2142 cm^{-1}. As in the case of methanol, CO formation in the DRIFTS cell also followed the same trends observed in the fixed bed reactor (Figure 1). Irrespective of the (mono- or bi-) metallic phase present on the surface, catalysts with a high concentration of adsorbed CO at reaction conditions (Pd, Pd/Ga(4.0), and Pd/Ga(1.0)) also presented a high rate of CO formation. This result evidences that both Pd and bimetallic Pd-Ga phases are active for RWGS reaction. As the Pd metallic sites are active for both desired and undesired reactions, the covering of surface metal palladium by Ga oxide as in Pd/Ga(0.2), Pd/Ga(0.5), and Pd/Ga(2.0) catalysts results in a decrease of the formation rates of methanol and CO when compared to those of the more pure Pd or Pd-Ga phases (Figure 1).

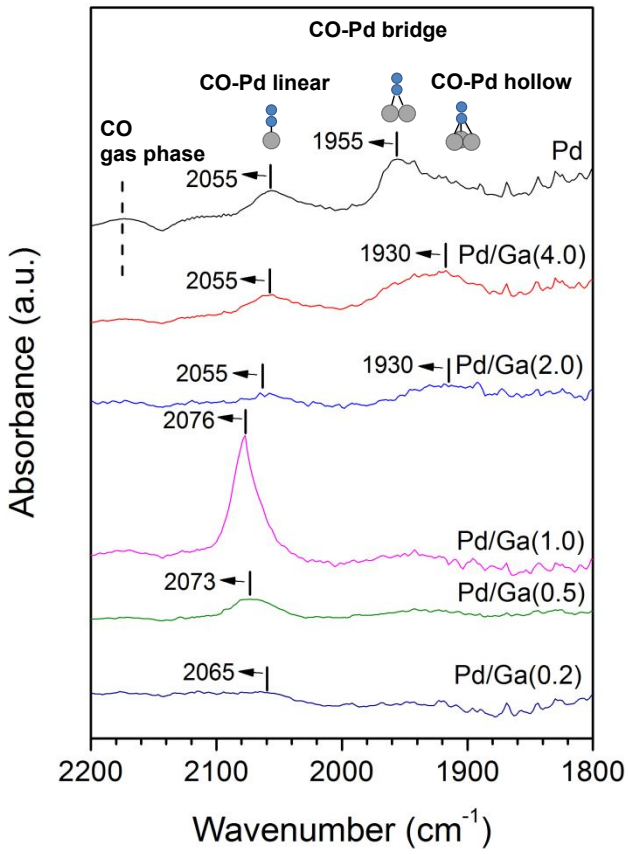

Figure 10. Operando DRIFTS results in the CO adsorption range (2200-1800 cm^{-1}) for all catalysts at reaction conditions: T = 240 °C, P = 400 kPa, H_2/CO_2 = 3.

In summary, a combination of a variety of characterization techniques and reactivity tests allowed us to describe the surface of Pd and Pd-Ga catalysts (represented in Scheme 1) and helped us to elucidate the nature of the most active sites for CO_2 hydrogenation to methanol. On Pd/Ga(4.0) and Pd/Ga(2.0) catalysts monometallic Pd phases were identified along with a Ga_2O_3 phase which was found to cover Pd sites decreasing their availability. Operando DRIFTS (Figure 9) confirmed that the active site responsible for methanol formation was Pd, which adsorbed bidentate formate species, the apparent primary intermediate in the formation of methanol via methoxy species. This result indicated that for catalyst samples with Pd/Ga > 2, the function of Ga in its oxidized form was to inhibit the activity of the catalyst by covering active sites thus, a synergistic effect between Pd and Ga_2O_3 was not evidenced (Scheme 1A).

For Pd/Ga(1.0), Pd/Ga(0.5), and Pd/Ga(0.2) catalysts, intermetallic Pd-Ga phases were formed. This fact was verified by XPS and operando DRITFS analyses showing the presence of an intermetallic Pd-Ga phase at reaction conditions. In the case of Pd/Ga(0.5) and Pd/Ga(0.2), the exact stoichiometry of the intermetallic was not discerned. Nevertheless, its capacity to increase the activity towards methanol production is evident, for Pd/Ga(0.5) methanol formation rate is one order of magnitude higher compared to catalysts with only monometallic Pd phase. As Ga content increased (lower Pd/Ga ratios),

a higher amount of surface Ga_2O_3 was evident which caused a decrease in the concentration of surface metallic sites. It is important to highlight that all of the promoted catalysts showed the presence of Ga_2O_3 on the surface, but only when an intermetallic phase was achieved a significant increase in activity towards methanol formation was observed. This finding was also consistent with previous reports [15, 17, 39]. This intermetallic phase was found to favor the hydrogenation rate of b-HCOO, which is a likely reaction intermediate in the methanol formation mechanism. Also, Figure 1 shows that increasing the amount of Ga decreases the conversion of CO_2, except in the case of Pd/Ga(1.0). were the catalyst surface was dominated by the presence of an intermetallic Pd_2Ga phase with minimum Ga excess thus resulting in a catalysts with the highest activity towards methanol formation (Scheme 1B). The surface characterization also allow us to postulate that a decrease in the reactivity of the bimetallic catalysts with increasing Ga content was due to the covering of Pd-Ga sites with an oxidized Ga phase (Scheme 1C). It is also important to note that a correlation exists between the metallic surface sites (probed by CO adsorption) and the increase in CO production which indicates that the monometallic and bimetallic phases of Pd are also active towards the formation of CO. However, the monometallic Pd sites do not favor the hydrogenation of formate to methoxy species, which makes them more selective towards the formation of CO.

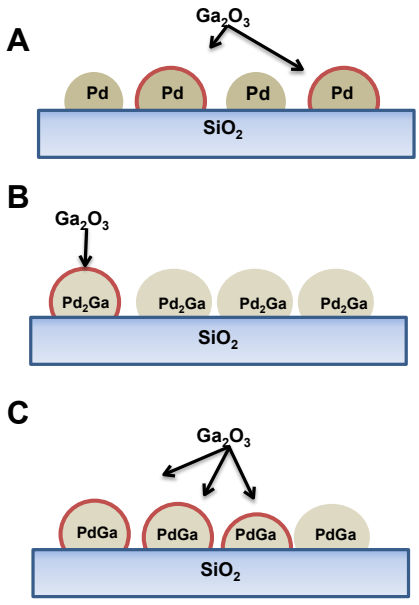

Low activity and selectivity to methanol:
- Pd/Ga(4.0)
- Pd/Ga(2.0)

Active and selective towards the formation of methanol:
- Pd/Ga(1.0)

Ga in excess creates layers of oxides on the surface that inhibit the reactivity of the catalyst:
- Pd/Ga(0.5)
- Pd/Ga(0.2)

Scheme 1. Graphical representation of the surface of the Pd-Ga catalysts during CO_2 hydrogenation conditions.

3. Conclusions

We showed that the existence of bimetallic Pd-Ga sites is necessary for boosting the rate of methanol formation in the synthesis of methanol from CO_2. Pd and Ga in separate phases

(Pd and Ga_2O_3) were not as active for methanol formation as it would be expected for catalysts with a strong synergistic effect between Pd and Ga_2O_3. A significant increase in the methanol formation rate and selectivity (up to 66%) was observed after promotion of Pd with Ga when compared to the unpromoted SiO_2-supported Pd catalyst. This was evidenced for defined Pd/Ga molar ratios (0.5 and 1.0). However, catalysts with relatively low Ga content (Pd/Ga molar ratios of 2.0 and 4.0) showed a catalytic performance similar to the Pd catalyst. We demonstrated through a combination of techniques including X-ray diffraction, STEM-EDS, CO-DRIFTS, quasi in situ XPS, and operando DRIFTS, the presence of bimetallic Pd-Ga phases in the most active and selective catalysts towards methanol formation. Operando DRIFTS showed that Pd or Pd-Ga metallic sites were responsible for the catalytic activity towards methanol via hydrogenation of formate (HCOO*) to methoxy species (CH_3O*). In this analysis, displacements towards lower wavenumber of υ_{as} (OCO) were observed for the catalysts where bimetallic phases were identified which correlated with a higher reactivity of surface bidentate formate species. These surface properties evidenced the different nature of the active sites and their higher hydrogenation rates to methanol with respect to the catalysts that present a monometallic Pd phase. Contrary to the finding for methanol formation active sites, both Pd and Pd-Ga sites were active for CO formation. Catalysts with a high loading of Ga in oxidized form suffered from blocking of active metallic sites, which decreased catalytic activity, as evidenced by the absence of surface formates on these catalysts.

Acknowledgments

The authors thank the government of Chile for the financing assigned through the following projects: FONDECYT 11140635, CONICYT PIA/APOYO CCTE AFB170007, CONICYT-PCI REDI170257 and Millennium Science Initiative of the Ministry of Economy, Development and Tourism, Chile, grant Nucleus on Catalytic Processes towards Sustainable Chemistry (CSC). Víctor G. Baldovino-Medrano thanks Fondo Nacional de Financiamiento para la Ciencia, la Tecnología y la Innovación Francisco José de Caldas and Agencia Nacional de Hidrocarburos for funding within the frame of the project No. 1102-721-50962. Saint-Gobain NorPro is acknowledged for kindly providing the SiO_2 support.

References

1. J. C. Medina, M. Figueroa, R. Manrique, J. Rodriguez Pereira, P. D. Srinivasan, J. J. Bravo-Suarez, V. G. Baldovino Medrano, R. Jimenez and A. Karelovic, *Catalysis Science & Technology*, 2017, **7**, 3375-3387.
2. I. Jbir, J. Couble, S. Khaddar-Zine, Z. Ksibi, F. Meunier and D. Bianchi, *Acs Catal*, 2016, **6**, 2545-2558.
3. J. K. A. Clarke, *Chemical Reviews*, 1975, **75**, 291-305.
4. S. E. Collins, J. J. Delgado, C. Mira, J. J. Calvino, S. Bernal, D. L. Chiavassa, M. A. Baltanas and A. L. Bonivardi, *J Catal*, 2012, **292**, 90-98.
5. G. A. Olah, *Angewandte Chemie International Edition*, 2005, **44**, 2636-2639.
6. C. Baltes, S. Vukojević and F. Schüth, *J Catal*, 2008, **258**, 334-344.
7. X. M. Liu, G. Q. Lu, Z. F. Yan and J. Beltramini, *Ind Eng Chem Res*, 2003, **42**, 6518-6530.
8. L. Fan and K. Fujimoto, *J Catal*, 1994, **150**, 217-220.

9. L. Fan and K. Fujimoto, *J Catal*, 1997, **172**, 238-242.
10. G. Wang, D. Mao, X. Guo and J. Yu, *International Journal of Hydrogen Energy*, 2019, **44**, 4197-4207.
11. T. Fujitani, M. Saito, Y. Kanai, T. Watanabe, J. Nakamura and T. Uchijima, *Applied Catalysis A: General*, 1995, **125**, L199-L202.
12. A. L. Bonivardi, D. L. Chiavassa, C. A. Querini and M. A. Baltanás, in *Studies in Surface Science and Catalysis*, eds. A. Corma, F. V. Melo, S. Mendioroz and J. L. G. Fierro, Elsevier, 2000, vol. 130, pp. 3747-3752.
13. D. L. Chiavassa, S. E. Collins, A. L. Bonivardi and M. A. Baltanás, *Chemical Engineering Journal*, 2009, **150**, 204-212.
14. J. L. Snider, V. Streibel, M. A. Hubert, T. S. Choksi, E. Valle, D. C. Upham, J. Schumann, M. S. Duyar, A. Gallo, F. Abild-Pedersen and T. F. Jaramillo, *Acs Catal*, 2019, **9**, 3399-3412.
15. E. M. Fiordaliso, I. Sharafutdinov, H. W. P. Carvalho, J. D. Grunwaldt, T. W. Hansen, I. Chorkendorff, J. B. Wagner and C. D. Damsgaard, *Acs Catal*, 2015, **5**, 5827-5836.
16. R. Manrique, R. Jiménez, J. Rodríguez-Pereira, V. G. Baldovino-Medrano and A. Karelovic, *International Journal of Hydrogen Energy*, 2019, DOI: https://doi.org/10.1016/j.ijhydene.2019.04.206.
17. A. Ota, E. L. Kunkes, I. Kasatkin, E. Groppo, D. Ferri, B. Poceiro, R. M. Navarro Yerga and M. Behrens, *J Catal*, 2012, **293**, 27-38.
18. A. Karelovic, G. Galdames, J. C. Medina, C. Yévenes, Y. Barra and R. Jiménez, *J Catal*, 2019, **369**, 415-426.
19. L. Liu, F. Fan, M. Bai, F. Xue, X. Ma, Z. Jiang and T. Fang, *Molecular Catalysis*, 2019, **466**, 26-36.
20. A. G. Saputro, R. I. D. Putra, A. L. Maulana, M. U. Karami, M. R. Pradana, M. K. Agusta, H. K. Dipojono and H. Kasai, *Journal of Energy Chemistry*, 2019, **35**, 79-87.
21. S. L. Soled, A. Malek, S. Miseo, J. Baumgartner, C. Kliewer, M. Afeworki and P. A. Stevens, *Studies in Surface Science and Catalysis*, 2006, **162**, 103-110.
22. S. H. Ali and J. G. Goodwin, *J Catal*, 1997, **171**, 333-338.
23. J. E. Benson, H. S. Hwang and M. Boudart, *J Catal*, 1973, **30**, 146-153.
24. M. A. Vannice, *Kinetics of catalytic reactions*, Springer, New York, 2005.
25. S. Grazulis, D. Chateigner, R. T. Downs, A. F. Yokochi, M. Quiros, L. Lutterotti, E. Manakova, J. Butkus, P. Moeck and A. Le Bail, *Journal of applied crystallography*, 2009, **42**, 726-729.
26. A. L. Patterson, *Physical Review*, 1939, **56**, 978-982.
27. V. Fernandez, D. Kiani, N. Fairley, F.-X. Felpin and J. Baltrusaitis, *Applied Surface Science*, 2020, **505**, 143841.
28. S. Krishnamoorthy, A. Li and E. Iglesia, *Catalysis Letters*, 2002, **80**, 77-86.
29. E. L. Kunkes, F. Studt, F. Abild-Pedersen, R. Schlögl and M. Behrens, *J Catal*, 2015, **328**, 43-48.
30. C. N. Satterfield, *Heterogeneous catalysis in industrial practice. 2nd edition*, New York, NY (United States); McGraw Hill Book Co., 1991.
31. R. Ladera, F. J. Pérez-Alonso, J. M. González-Carballo, M. Ojeda, S. Rojas and J. L. G. Fierro, *Applied Catalysis B: Environmental*, 2013, **142-143**, 241-248.
32. R. van den Berg, G. Prieto, G. Korpershoek, L. I. van der Wal, A. J. van Bunningen, S. Lægsgaard-Jørgensen, P. E. de Jongh and K. P. de Jong, *Nature Communications*, 2016, **7**, 13057.
33. R. van den Berg, G. Prieto, G. Korpershoek, L. I. van der Wal, A. J. van Bunningen, S. Laegsgaard-Jorgensen, P. E. de Jongh and K. P. de Jong, *Nat Commun*, 2016, **7**, 13057.
34. R. A. Van Santen, *Accounts of Chemical Research*, 2009, **42**, 57-66.

35. N. Sheppard and C. De La Cruz, *Catal Today*, 2001, **70**, 3-13.
36. K. Zorn, S. Giorgio, E. Halwax, C. R. Henry, H. Grönbeck and G. Rupprechter, *The Journal of Physical Chemistry C*, 2011, **115**, 1103-1111.
37. K. Kovnir, M. Armbrüster, D. Teschner, T. V. Venkov, L. Szentmiklósi, F. C. Jentoft, A. Knop-Gericke, Y. Grin and R. Schlögl, *Surface Science*, 2009, **603**, 1784-1792.
38. G. Wowsnick, D. Teschner, I. Kasatkin, F. Girgsdies, M. Armbrüster, A. Zhang, Y. Grin, R. Schlögl and M. Behrens, *J Catal*, 2014, **309**, 209-220.
39. K. Föttinger and G. Rupprechter, *Accounts of Chemical Research*, 2014, **47**, 3071-3079.
40. S. Penner, H. Lorenz, W. Jochum, M. Stöger-Pollach, D. Wang, C. Rameshan and B. Klötzer, *Applied Catalysis A: General*, 2009, **358**, 193-202.
41. N. Iwasa, S. Masuda, N. Ogawa and N. Takezawa, *Applied Catalysis A: General*, 1995, **125**, 145-157.
42. G. Schön, *Journal of Electron Spectroscopy and Related Phenomena*, 1973, **2**, 75-86.
43. N. Winkler, R. A. Wibowo, W. Kautek, G. Ligorio, E. J. W. List-Kratochvil and T. Dimopoulos, *Journal of Materials Chemistry C*, 2019, **7**, 69-77.
44. Z. Hou, Y. Liu, J. Deng, Y. Lu, S. Xie, X. Fang and H. Dai, *ChemCatChem*, 2018, **10**, 5637-5648.
45. C. Rameshan, W. Stadlmayr, S. Penner, H. Lorenz, L. Mayr, M. Hävecker, R. Blume, T. Rocha, D. Teschner, A. Knop-Gericke, R. Schlögl, D. Zemlyanov, N. Memmel and B. Klötzer, *J Catal*, 2012, **290**, 126-137.
46. A. Haghofer, K. Föttinger, F. Girgsdies, D. Teschner, A. Knop-Gericke, R. Schlögl and G. Rupprechter, *J Catal*, 2012, **286**, 13-21.
47. J. Osswald, K. Kovnir, M. Armbrüster, R. Giedigkeit, R. E. Jentoft, U. Wild, Y. Grin and R. Schlögl, *J Catal*, 2008, **258**, 219-227.
48. X. Jiang, X. Wang, X. Nie, N. Koizumi, X. Guo and C. Song, *Catal Today*, 2018, **316**, 62-70.
49. G. C. Cabilla, A. L. Bonivardi and M. A. Baltanás, *Applied Catalysis A: General*, 2003, **255**, 181-195.
50. J. Nakamura, Y. Choi and T. Fujitani, *Topics in Catalysis*, 2003, **22**, 277-285.

Pd/Ga ratio influences the phases formed during catalysis. The best catalyst necessitates the formation of Pd-Ga intermetallic compounds and also low content of Ga_2O_3, whose excess tend to block surface sites.